WOOD-CHAR GASIFICATION: EXPERIMENTS AND ANALYSIS ON SINGLE PARTICLES AND PACKED BEDS

S. DASAPPA [1], P. J. PAUL[2], H. S. MUKUNDA[2] and U. SHRINIVASA[3]

[1] Centre for ASTRA
[2]Department of Aerospace Engineering
[3] Department of Mechanical Engineering
Indian Institute of Science
Bangalore 560 012, India

Introduction

Gasification has been studied with the aim of designing reactors, gasifiers, and other combustion systems. In a cocurrent gasifier [1], air and solid fuel move in the same direction, and the flame front moves in the opposite direction. Air first reacts with the solid fuel either in the heterogeneous mode (e.g., in the case of a charcoal gasifier) or with the volatiles generated from the solid fuel in the gas phase, releasing heat and helping in the propagation of a flame front into the unreacted solid aided by axial heat transfer by conduction and radiation. The hot combustion products (CO_2 and H_2O) are further reduced by the char. These endothermic reactions generate carbon monoxide and hydrogen, and the exit gas can be utilized as a gaseous fuel. Similar processes also occur during fire spread in permeable materials. A number of workers [2–4] have examined the propagation rate of a flame front against airstream through a packed bed of solids such as wood, foam, or biomass. The primary emphasis in these studies has been in predicting the flame spread through the media. Only the first process described earlier, namely, the oxidation, is of importance in predicting the flame spread rate. However, for design and operation of a gasifier, both oxidation and reduction processes are of equal importance. Hence, the present paper is aimed at studying these processes in an isolated single particle and extending the results to a bed of particles to predict the various features of an operating gasifier, namely, the flame front movement, the profiles of different species concentrations and temperature, and the exit gas composition from the gasifier. The present work is limited to charcoal gasification only. The model developed would be of use for understanding and designing biomass gasifiers.

Several designs of wood gasifiers exist [1,5–7], with modeling aspects addressed by a few [5,8,9] using overall kinetics in a packed bed. Predictions are compared with experiment results by tuning several kinetic and bed-related parameters.

The wood char reactions in CO_2–N_2 mixtures and O_2–N_2 mixtures have been studied in detail in our earlier studies [10,11]. The steam–carbon reaction has been studied by several researchers in the late 1940's and early 1950's [12–14] for extracting suitable rate expression. Kinetic expressions of varying complexity have been derived by these researchers [14–17] for steam–carbon reaction at temperatures of 1200 to 1500 K and in an environment of mixtures including CO, CO_2, and O_2. Satyanarayana and Keairns [15] have conducted experiments on char gasification using CO_2 andH_2O. They show from the results that the rate constants of the C–H_2O reaction are about 2.5–5 times faster than of the C–CO_2 reaction.

The Experiments

Single-Particle Char Experiments

The experimental setup consists of a 40-mm-diameter quartz reactor placed in a temperature-controlled furnace [11] through which measured flow of gases consisting of H_2O, CO_2, O_2 , and N_2 in the desired proportions are passed, as shown in

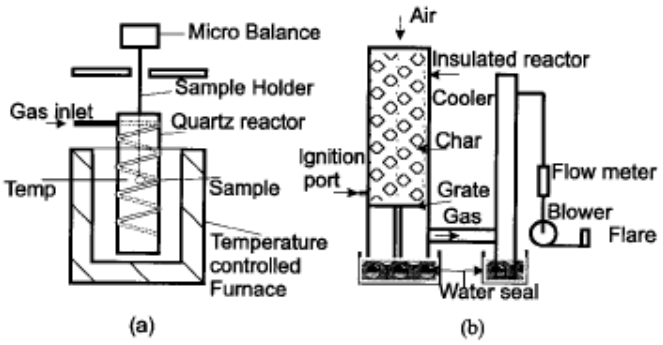

Fig. 1. Experimental setup for single char particle and the packedbed reactor.
(a) Single-particle experimental setup. (b) Packed-bed reactor.

Fig. 1. Preparation of the char samples (of 4–15 mm diameter from Ficus wood), their characterization for porosity, and the other experimental aspects including the qualitative behavior of conversion are the same as in the earlier work on C–CO_2 conversion [11]. The present experiments were conducted at 1250 and 1390 K to extract the temperature effect on the conversion rate.

Experiments with Packed Bed

For measuring the propagation rates, experiments similar to those performed by Reed and Markson [8] were conducted. A 65-mm-diameter and 300-mmhigh quartz reactor insulated with an observation slit 10 mm wide throughout the length was used as shown in Fig. 1. This corresponds to 1/40 scale version of the state-of-art wood gasifier of 275 kW (thermal) [18]. The other elements used are similar to the commercial large gasifier—a grate to hold the charge and tubing to draw the gas to the cooler through a blower into a flare. Charcoal pieces of approximately cubical, 8 mm size were used in the experiments. After initial light-up through the ignition port above the grate, the system was run at fixed flow rates, and the rate of progress of the flame front upward was measured. It was observed that the glowing zone was approximately 25 to 35 mm (3–4 particle depth) and the peak bed temperature measured was in the range of 1000–1230 K depending upon the mass flux.

The Model

The modeling is done in two parts: for the single particle and for the packed bed of particles. The model for single particle is similar to the earlier work [10] with some minor modifications for representing particles at different heights in a packed bed. The additional equations to be solved are for axial transport of heat and mass through the bed.

Single-Particle Modeling

The processes taking place during the combustion or gasification of porous carbon spheres are diffusion and convection of the species and energy in the porous medium and heterogeneous reaction between the gaseous species and the char. These are modeled using unsteady, spherically symmetric one-dimensional conservation equations for species and energy [11,10]. The representative equation for a species is

$$\frac{\partial(\rho\varepsilon Y_i)}{\partial t} = \frac{1}{r^2}\frac{\partial}{\partial r}\left(-\rho v r^2 Y_i + r^2 D_e \rho \frac{\partial Y_i}{\partial r}\right) + \dot{\omega}_i''' \quad (1)$$

where $\rho = \rho_c(1 - \varepsilon) + \rho\varepsilon$ is the average density of porous char, ρ_c is nonporous char density, ε is the porosity of the char, and ω''' is the volumetric reaction rate of specie *i* due to the heterogeneous reactions with the internal surface of the porous char and the gas-phase reactions in the pores. The reaction rates of CO_2 and O_2 with char

have been discussed and validated earlier [11, 10].

The surface reaction rate of carbon with steam is given by Blackwood and McGrory [14],

$$\dot{\omega}''' _{C_{H_2O}} = -\frac{k_1 p_{H_2O} + k_4 p_{H_2} p_{H_2O} + k_5 p^2_{H_2O}}{1 + k_2 p_{H_2} + k_3 p_{H_2O}} \quad (2)$$

The water gas shift reaction,

$$CO + H_2O \rightleftharpoons CO_2 + H_2$$

is assumed to be in equilibrium within the pores [5,9,1]. Blackwood and McGrory [14] showed that the presence of even a small fraction of ash helps in the generation of CO_2 during steam gasification by catalyzing the water–gas reaction.

Boundary conditions for the foregoing conservation equations are obtained by considering the heat and mass transfer in the gas film surrounding the char sphere [11]; these take into account free and forced convection and net mass flow out of the sphere surface. Heat radiation from the surface of the sphere is also accounted for.

The equations are solved using finite-difference procedure, and the results of profiles of species concentration, temperature, and porosity as functions of time are obtained. The results are compared with the experimentally obtained mass loss rate and temperatures at fixed locations in the sphere.

Modeling of Particles in Packed Bed

The single-particle model described earlier can be extended to modeling a packed bed of particles discussed in the section Experiments with Packed Bed. The bed is divided into a number of computational cells, and conservation equations for a typical particle representing each cell are solved. Two additional features in the boundary conditions need to be considered for a particle in a bed compared to the single particle, namely, the heat transfer between the particle and the surrounding particles, and the other is the properties of the bulk fluid surrounding the particles that vary continuously. These are determined by solving a set of conservation equations for the bulk gases assuming variations only with the height of the bed. With coordinates fixed to the particles, the conservation equations can be written as

$$\frac{\partial \dot{m}''}{\partial x} = n\dot{m}_p \quad (3)$$

$$\frac{\partial(\varepsilon_b \rho Y_i)}{\partial t} + \frac{\partial \dot{m}'' Y_i}{\partial x} = \frac{\partial}{\partial x} D\rho \frac{\partial Y_i}{\partial x} + n[\dot{m}_p Y_{i,s} + K_D(Y_{i,s} - Y_i)] + W'''_i \quad (4)$$

$$\frac{\partial(\varepsilon_b \rho c_p T)}{\partial t} + \frac{\partial(\dot{m}'' c_p T)}{\partial x} = \frac{\partial}{\partial x} k_{eff} \frac{\partial T}{\partial x} + n[\dot{m}_p c_p T_s + hA_s(T_s - T)] + H_R \quad (5)$$

where n is the number of particles per unit volume, ε_b is the bed porosity, m_p is the gasification rate of one particle, m'' is the superficial mass flux of the gases of the bed, K_D and h are the mass and heat transfer coefficients, respectively, through the gas film surrounding the particle [11], and W''' and H_R are the gas-phase reaction rate and the heat generation rate due to gas-phase reactions, respectively.

The subscript s denotes the properties at the surface of the particle. For calculating ε_b, the particles are considered to be nonporous. The internal porosity of the particles are considered separately when solving for individual particles. In the continuity equation 3, the time derivative term has been neglected.

For handling particle-to-particle heat transfer, it is assumed that radiation is the major mode of heat exchange among particles [19, 8, 9]. Conduction is likely to play only a minor role because the area of contact between particles is small in randomly packed bed, and emissivity of char particles is large (close to unity). A particle views the surrounding particles at various heights with different temperatures. To account for this, the surface of the particle is divided into strips of latitudes of width $\delta\Theta$. It is assumed that view factor f_j of the sphere with all the particles whose centers reside in the

latitudinal width *dh* is equal to the ratio of the area of the strip to the total surface area of the sphere. All such particles are assumed to have a uniform surface temperature representing the average height at which these particles reside within the bed. Assuming further that emissivities of all the surfaces are equal, the total radiative flux falling on the sphere and the net radiation absorbed can be obtained as

$$Q = \sum_j f_j \sigma T_j^4 \qquad (6)$$

$$H_R = A_s \alpha (Q - \sigma T_s^4) \qquad (7)$$

where A_s is the surface area of the sphere and $\propto$ the absorptivity (or emissivity) of the surface. To determine T_j, it is assumed that the particle views, on average, other particles at a center-to-center distance of a constant multiple of the particle diameter. This effective distance can be different from the average center-to-center distance of the particles in the bed because of the T^4 relationship for radiation and due to the nonuniformity of the surface temperature of a sphere. From the data on the effective thermal conductivity of packed beds due to radiation [19], it has been estimated as 0.65*d*.

The solution of equations for packed beds is performed using a time-split technique. The initial condition is ambient temperature for all the particles in the bed except for some cells near the bottom for which higher temperatures are assigned for ignition. In the first fractional time step, conservation equations for the porous sphere are solved (equation 1). Local conditions of the gas form the boundary conditions for the reacting porous spheres. One representative sphere is solved for each computational cell along the height of the bed. Solution of the equations for the particle gives the conditions at the surface of the sphere and the net mass flow from the sphere surface, which are used in the next fractional time step when equations 3–5 are solved.

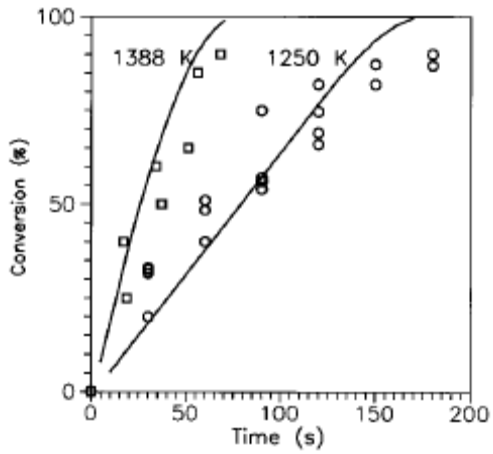

Fig. 2. Variation of conversion with time—experiments (points) and predictions (line) for d_o = 8 mm and T_{amb}=1250 K and 1388 K.

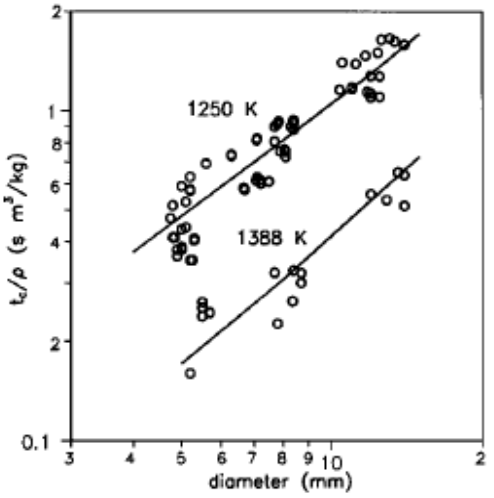

Fig. 3. Normalized conversion time versus d_0—experiments and predictions for T_{amb} 4 1250 and 1388 K.

Choice of Parameters

The choice of physical, thermodynamic, and transport properties is based on the mean char properties presented as follows:

Q_c 4 1900 kg/m3
R_p (*t* 4 0) 4 50 *l*m
c_p 4 1.25 kJ/kg K
H_c 4 32.60 MJ/kg
K_c 4 1.85 W/m K

Rate parameters for C +H_2O reaction are

k_1 = 3.7 2 10^7exp(130,000/*T*) mol/cm3atm
k_2 = 35 atm^{-1}
k_3 = 2.1 * 10^{-3} exp(-10,055/*T*) atm^{-1}
k_4 = 91.8 exp(-15,083/*T*) atm^{-1}

$k_5 = 2.5 * 10^{-8}$ atm^{-1}

The porous char conductivity is 0.4–0.5 W/m K [20,21] and accounts for conduction and radiation inside the char. The thermal conductivity of the gas phase, k_g, is calculated locally taking into account the presence of hydrogen. Conductivity of the mixture increases by a factor of 1.2–1.5 with the addition of 10% H_2 in the mixture [22]. The initial porosity of the wood char considered is in the range of 0.75–0.85, consistent with the present measurements as well as those of Groeneveld [5]. The initial radius of the pore is obtained from Groeneveld [5] where wood char was used for measurements. The parameters in the kinetic expression used presently are obtained from Blackwood and McGrory [14]. The rate constant of the backward reaction, k_2, is obtained from the appropriate equilibrium constants. The emissivity in the expression for radiant heat loss is taken at 0.95. Following earlier work for the packedbed [9], bed porosity is chosen at 0.5, consistent with the randomly packed system [19]. The heat loss coefficient from the reactor to the ambient is estimated from the model reactor experiments as 6 W/m^{2}K.

Results and Discussion

Figure 2 shows the results of char conversion (X_c) with time for an 8-mm-diameter char particle at two different ambient temperatures. Char conversion is the ratio of the difference between the initial weight and weight at any time t to the initial weight. The parameters that influence the conversion time curve are the activation energy and the char conductivity. Activation energy affects the initial slope, whereas the conductivity affects the point at which the curve departs from the linearity. Because gas-phase conductivity is calculated depending on the local gas composition and temperature, activation energy is the only parameter that is uncertain. The suggested value of activation energy from Blackwood and McGrory is 121 kJ/mole obtained from experiments on coconut char. Using the experimental results at two different temperatures 1250 and 1388 K, the activation energy was evaluated. The scatter in the experimental data is due to inherent structural differences in wood. Because of this feature, the predictions can be taken to be in reasonable agreement with the experimental results at an activation energy of 212 kJ/mole, matching closely with Groeneveld's [5] experimental results for wood char (217 kJ/mole). This comparison supports the choice of kinetic and transport parameters chosen for the model.

Figure 3 shows the experimental data and the prediction of burn time normalized with respect to density of char with initial char diameter for combustion

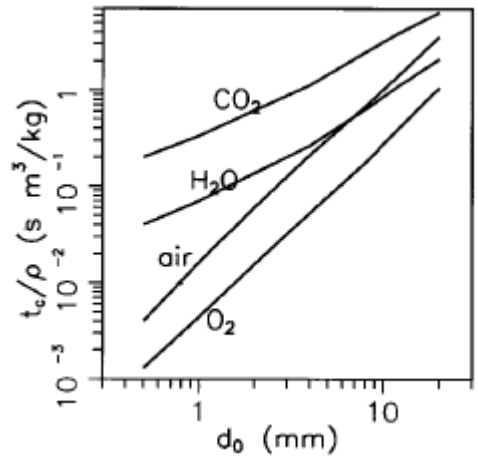

Fig. 4. Normalized conversion time versus diameter for different reactants at T_{amb} = 1273 K.

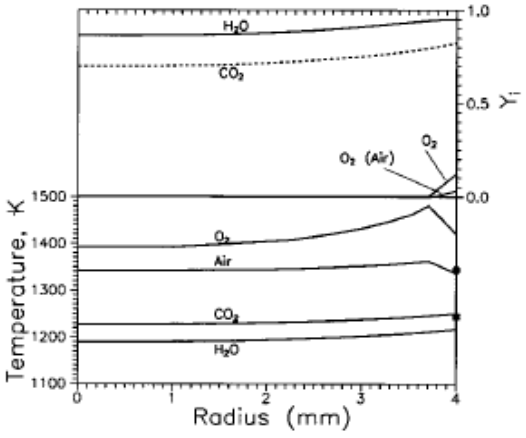

Fig. 5. Temperature and reactant profile inside an 8-mm-diameter reacting particle at T_{amb} = 1273 K with different reactants. Measured surface temperature with CO_2(square) and air (circle) are also shown.

at two different temperatures on a log–log plot. The experimental results were restricted to a particle diameter range of 4–15 mm. The results show a conversion time dependence on the diameter as t_c ; at 1250 K and at 1388 K. $d^{10.2}$ $d^{10.3}$ These results indicate the departure from the diffusion-controlled d^2 law. The model predication on the diameter dependence at the two temperatures compares well with the experimental data. These results further confirm the choice of kinetic and transport parameters. The conversion time–diameter correlations are summarized by

$$t_c/\rho = d_0^{T/1050} \exp\left[-3.26 + 15470\left(\frac{1}{T} - \frac{1}{1273}\right)\right] \quad (8)$$

with t_c in s, q in kg/m^3, d_0 in mm, and T in K. The indication of higher reactivity and a shift toward a diffusion-limited condition.

Figure 4 shows comparative data on the conversion time versus diameter for various reactants at 1273 K. The diameter dependence is nearly d^2 in case of pure oxygen and air environment, indicating the diffusion-dominated exothermic char conversion. The conversion time for CO_2 ambient is about 3.5 times that of H_2O ambient, comparing well with the results of Satyanarayana and Keairns [15]. The consumption rate of char in H_2O ambient is comparable or higher than that of char in air beyond a particle diameter of 8 mm. The results for CO_2 and H_2O show lower slopes than those for air, and therefore, the process is controlled by both diffusion and chemical reaction. Further, kinetic dominance increases with the reduction in particle diameter below 4 mm.

Figure 5, showing the temperature and reactant profile inside the particle, is used to examine the thermochemical behavior with different reactants. Temperature is highest for O_2, followed by air and CO_2, and lowest for H_2O. The reaction between oxygen and char is exothermic, and hence, char temperature is higher than ambient for oxygen and air. Consistent with the relative reactivities, pure oxygen creates higher char temperature than air. H_2O and CO_2 reactions with char are endothermic, and consequently, the temperatures within the char are below ambient. Further, the variation in temperature through the particle is highest for O_2 and lowest for CO_2. This difference is due to the diffusion-controlled process for O_2 and significantly reaction-controlled process in the case of CO_2. In the case of O_2 and air, the mass fraction of oxygen becomes close to zero at the surface, and in the case of H_2O and CO_2, the mass fraction at the core is a significant fraction of that at the surface. The relatively lower slope for H_2O compared to CO_2 is due to higher diffusivity of the gas reacting inside the sphere for H_2O. The ratio of reaction rates between surface and core demonstrates the combined effects of temperature and reactant distribution described earlier. The ratio exceeds by a factor of 10^4 for O_2 and air and is of the order of unity (2, in fact) for both H_2O and CO_2.

Calculations were made for the dependence of the reactant mass fraction (with inert being the other component) on char conversion time. These dependencies can be described by $t_c/\rho \sim X_{O2}^{-1}$, $X_{CO2}^{-0.65}$, and $X_{H2O}^{-0.7}$, respectively. For high-temperature environment, the relative conversion times are described by the following relations:

$$\left(\frac{t_c}{\rho}\right)_{CO_2} = d_0^{1.05} \cdot \exp\left[-1.715 + 35{,}300\left(\frac{1}{T} - \frac{1}{1273}\right)\right] X_{CO_2}^{0.65} \quad (9)$$

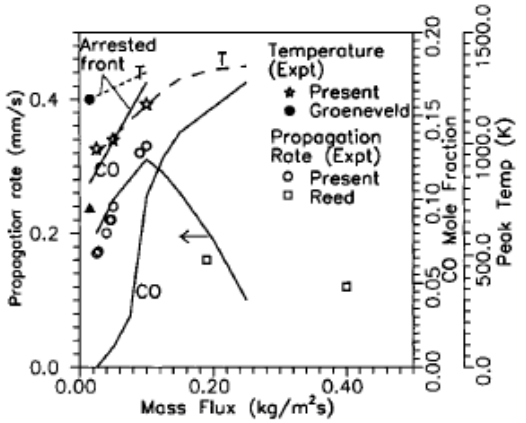

Fig. 7. Experimental and model predictions on the propagation rate versus mass flux in a packed-bed char reactor along with peak bed temperature and CO concentration. Also shown are the measured [5] and predicted values of CO

(filled triangle) and peak temperature (filled circle) for arrested flame propagation. Points indicate experimental data, and lines are predictions.

$$\left(\frac{t_c}{\rho}\right)_{H_2O} = d_0^{T/1050} \cdot \exp\left[-3.26 + 15{,}470\left(\frac{1}{T} - \frac{1}{1273}\right)\right] X_{H_2O}^{0.70} \quad (10)$$

$$\left(\frac{t_c}{\rho}\right)_{O_2} = 0.0022 d_0^{3} X_{O_2}^{-1.0} \quad (11)$$

In the foregoing equations, t_c is in s; ρ, the density of the particle, is in kg/m^3; d_0, the diameter of the particle, is in mm; T, the ambient temperature, is in K; and X_i is the mole fraction of species i. The previous correlation is accurate to 510% and is valid for the following range of parameters: d_0>4 mm, T = 1000–1400 K, X_i < 0.3.

Propagation rate in packed bed

The profiles of temperature and mole fractions of CO and CO_2 at three different mass fluxes are shown in Fig. 6. The profiles are chosen at a time when the rate of propagation of the reaction front through the bed is constant. It can be seen that the peak temperature increases as the air mass flux increases. It is also evident that the thickness of the propagation front increases with air flux, which is consistent with the qualitative observations during the present experiments and earlier references [5]. At very low air fluxes, CO is not generated at any significant levels. At larger fluxes, the level of CO concentration in the exit gas increases.

Figure 7 shows the variation of propagation rate of the reaction front in a packed bed of char with the superficial air mass flux through the bed. The experimental results from the present work and from those of Reed and Markson [8] are also included in the same figure.With increase in mass flux, the front velocity initially increases and then reduces, indicating the balance on the heat and mass transfer limitations during the process. The peak temperature and the exit CO mole percent are also plotted. As can be seen, CO content in the gas is very small at low air mass flux, and both the peak temperature and CO content in the exit increase with air mass flux. These results are different from those of Fathehi and Kaviany [3], who obtain the maximum temperature and maximum front velocity at nearly the same air mass flux. The major difference is that they [3] used a bed material with high volatile content, and a major part of this fuel is consumed while the reaction front passes through the fuel. In contrast, in the present case of charcoal, only a small fraction of the fuel is consumed in the reaction front, and the situation is fuel rich in all cases. The reaction front heats up much more fuel than it consumes, and this limits the maximum temperature achieved at the flame front. Because the rate of increase of front velocity with air mass flux is much less than the rate of increase of air mass flux itself, the peak temperature at the front increases with air mass flux, also aided by the increased heat and mass transfer coefficients between the particle and gas. However, at large air mass flux, the convective cooling of the reactant front reduces the propagation rates even though the temperature of the front keeps increasing. The model predictions in this ranges of flux agree well with the present experiments and that of Reed and Markson [8].

Groeneveld [5] conducted experiments in a reactor with 0.3 m diameter with wood char bed at an air flux of 0.015 kg/m^2 s and reported exit CO mole fraction of about 10% and the peak bed temperature of 1200 K. Such high temperature is not obtained in a propagating flame front because of the reasons described in the previous paragraph. However, when air is provided through a distributor in the middle of the bed, the front does not propagate beyond this point. Since the front is arrested at this point, the front temperature increases to much higher value compared to the propagating front at the same air flux, because the amount of unburned char being heated becomes limited. Figure 7 also contains data for such a situation along with the experimental data of Groeneveld [5]. It can be seen that peak temperature and CO mole fraction are increased significantly in an arrested front compared

to the propagating front. The lone experimental data point of Groeneveld [5] shows good match with the predictions.

Conclusions

Char gasification, which forms an important part of biomass gasification, has been modeled. The reactions of char with O_2, CO_2 , and H_2O have been studied independently on single particles, and a model for these has been developed and validated for different ambient temperatures, compositions, and external convection. The model has been extended to packed bed of particles, which has also been validated with the present and previous experiments. The model can be used for understanding and designing biomass gasifiers.

Nomenclature

A_s surface area of the particle (m_2)

d_0 initial diameter (m)

$E_{1,2}$ activation energy (J/mol)

H_c heat of combustion of carbon (J/kg)

k, k_c, $\bar{k}$ thermal conductivity of gas, carbon, and porous char (W/m K)

k_1–k_4 rate constants

M_i molecular mass of species i

$\dot{m}$ 9 superficial mass flux in the bed (kg/m_2 s)

n number of particles per unit volume of the bed

p pressure (Pa)

r radial coordinate (m)

R universal gas constant (J/kg mol K)

t time (s)

T temperature (K)

u_p velocity of movement of the char bed (m/s)

x_c fraction of char consumed

x distance (m)

Y_i mass fraction of species i
q density of gas (kg/m_3)

e_b bed porosity

a absorptivity of the surface

$\dot{x}_i$- volumetric reaction rate, equation 2 (kg/m_3 s)

REFERENCES

1. Reed, T. B., Graboski, M. S., and Levie, B., *Fundamentals, Development and Scaleup of the Air-Oxygen Stratified Downdraft Gasifier,* The Biomass Energy Foundation Press, Golden, CO, 1988.

2. Dosanjh, S. S., Pagni, P. J., and Fernandez-Pello, A. C., *Combust. Flame* 68:131–142 (1987).

3. Fathehi, M. and Kaviany, M., *Combust. Flame* 99:1–17 (1994).

4. Ohlemiller, T. J., Bellan, J., and Rogers, F., *Combust.Flame* 36:197–215 (1979).

5. Groeneveld, M. J., "The Co-current Moving Bed Gasifier," Ph.D. thesis, Twente University of Technology, Netherlands, 1980.

6. Walawander, W., Chern, S. M., and Fan, L. T., in *Fundamentals of Thermo-chemical Biomass Conversion,* pp. 911–922. Elsevier Applied Science, New York, 1985.

7. Kaupp, A. and Goss, J., *Final report to USDA, Forest Service, Contract 53-319 R-0-141,* March 1981.

8. Reed, T. B. and Markson, M., in *Proc. of the Fifteenth Biomass Thermochemical Conversion Contractors Meeting,* Atlanta, GA, 1983, pp. 217–254.

9. Basak, A. K., "*Modeling of a Downdraft Charcoal Gasifier,*" Master's thesis, Asian Institute of Technology, Thailand, 1985.

10. Dasappa, S., Sridhar,H. V., Paul, P. J., Mukunda, H. S., and Shrinivasa, U., in *Twenty-Fifth Symposium (International) on Combustion,* The Combustion Institute, Pittsburgh, 1994, pp. 1619–1628.

11. Dasappa, S., Paul, P. J., Mukunda, H. S., and Shrinivasa, U., *Chem. Eng. Sci.* 49-2:223–232 (1994).

12. Gadsby, J., Hinshelwood, C., and Sykes, K. W., *Proc. R. Soc.* A187:129–151 (1946).

13. Long, F. J. and Sykes, K., *Proc. R. Soc.* A193:377–399 (1948).

14. Blackwood, J. D. and McGrory, F., *Aust. J. Chem.* 11:16–23 (1958).

15. Satyanarayana, K. and Keairns, D. L., *Ind. Eng. Chem. Fundamentals* 20:6–13 (1981).

16. Shaw, J., *Fuel* 56:134–129 (1977).

17. Mulhen, H. J., Heek, K. H., and Juntgen, H., *Fuel* 64:944–949 (1985).

18. Mukunda, H. S., Dasappa, S., Paul, P., and Shrinivasa, U., "Energy for Sustainable Development," *J. Int. Energy Initiative* 1(3):27–38 (1994).

19. Gabor, J. and Bollerill, J., *Handbook of Heat Transfer Applications,* (Warren M. Rohsenow, James P. Hartnett, and Ejup N. Ganic, eds.) McGraw-Hill, New York, 1985.

20. Gabor, J. and Bollerill, J., *Gas Engineers' Handbook,* McGraw-Hill, New York, 1934.

21. Goldman, J., Xieu, D., Oko, A., Milne, R., and Essenhigh, R. H., in *Twentieth Symposium (International) on Combustion,* The Combustion Institute, Pittsburgh, 1984, pp. 1365–1372.

22. Kanury, A. M., *Introduction to Combustion Phenomena,*Gordon and Breach Science Publishers, Amsterdam, 1982.